Supporting Information

Liposomal Delivery of Mitoxantrone and a Cholesteryl Indoximod Prodrug Provides Effective Chemo-Immunotherapy in Multiple Solid Tumors

Kuo-Ching Mei[1, 2], Yu-Pei Liao[1,2], Jinhong Jiang[2], Michelle Chiang[2], Mercedeh Khazaieli[2], Xiangsheng Liu[1,2], Xiang Wang[2], Qi Liu[2], Chong Hyun Chang[2], Xiao Zhang[1], Juan Li[1], Ying Ji[1], Brenda Melano[2], Donatello Telesca[3], Tian Xia[1, 2], Huan Meng[1,2,4]* and Andre E. Nel[1,2,4]*

1 Division of NanoMedicine, Department of Medicine, David Geffen School of Medicine University of California, Los Angeles, California, 90095, United States

2 California NanoSystems Institute, University of California, Los Angeles, California 90095, United States

3 Department of Biostatistics, University of California, Los Angeles, California, 90095, United States

4 Jonsson Comprehensive Cancer Center, University of California, Los Angeles, California, 90095, United States

Correspondence should be addressed to:

Andre E. Nel, Division of NanoMedicine, Department of Medicine, University of California, Los Angeles, 52-175 CHS, Los Angeles, California 90095, USA. Phone: 310.825.6620; E-mail: anel@mednet.ucla.edu;

Huan Meng, Division of NanoMedicine, Department of Medicine, University of California, Los Angeles, 570 Westwood Plaza, Building 114, Room 6511, Los Angeles, California 90095, USA. Phone: 310.825.0217; E-mail: hmeng@mednet.ucla.edu.

Table of Content

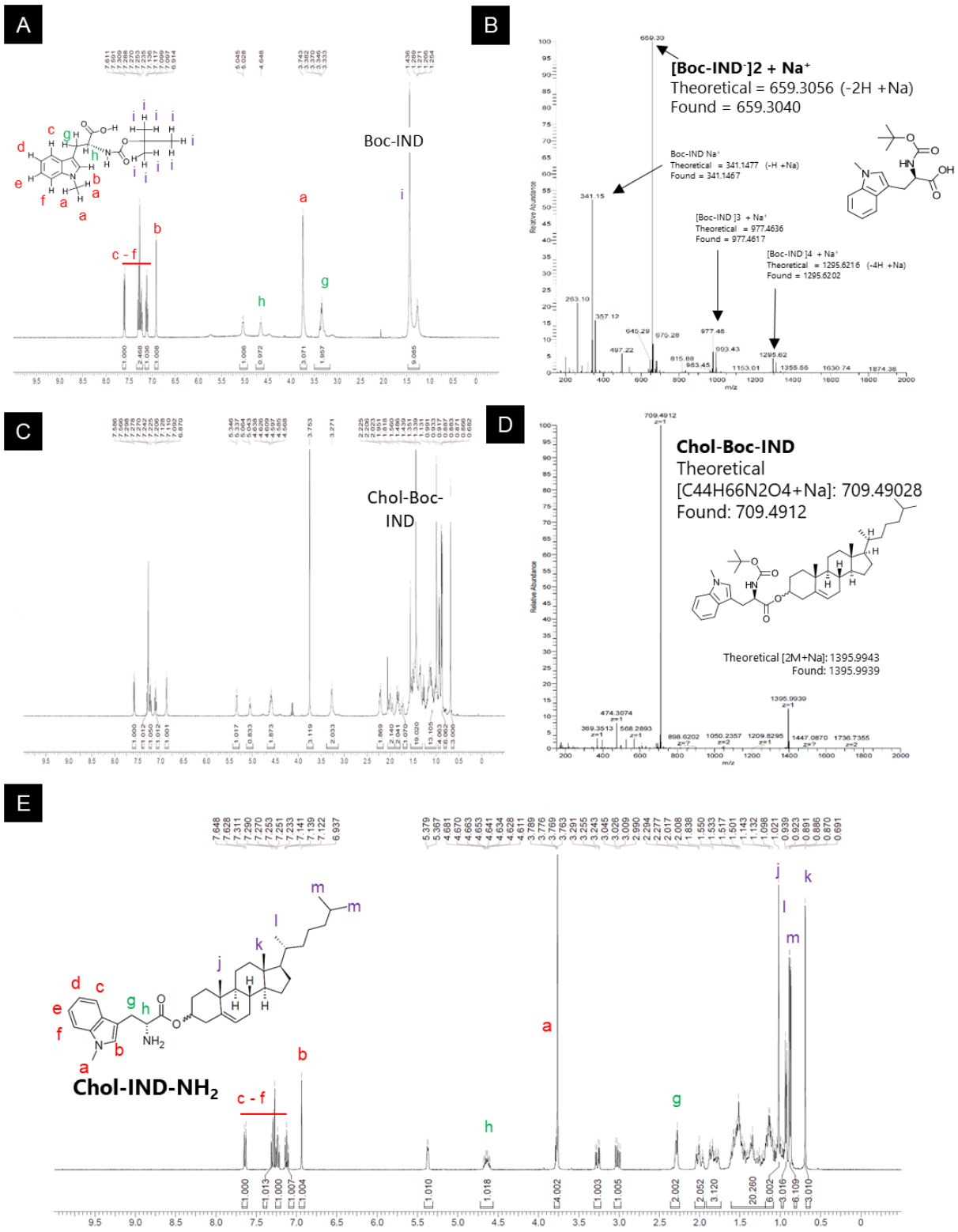
A
Boc-IND
B
[Boc-IND⁻]2 + Na⁺
Theoretical = 659.3056 (-2H +Na)
Found = 659.3040
Boc-IND Na⁺
Theoretical = 341.1477 (-H +Na)
Found = 341.1467
[Boc-IND]3 + Na⁺
Theoretical = 977.4636
Found = 977.4617
[Boc-IND]4 + Na⁺
Theoretical = 1295.6216 (-4H +Na)
Found = 1295.6202
C
Chol-Boc-IND
D
Chol-Boc-IND
Theoretical
[C44H66N2O4+Na]: 709.49028
Found: 709.4912
Theoretical [2M+Na]: 1395.9943
Found: 1395.9939
E
Chol-IND-NH2

Figure S1. NMR and MS spectra to confirm successful cholesteryl-indoximod synthesis.

(A) Boc-IND (6.50 g, 20.2 mmol, 88.4% yield, 99.2% purity) was obtained as a white solid, which was confirmed by ^{1}H NMR 400 MHz, CDCl3: δ 7.60 (d, J = 8.0 Hz, 1H), 7.20 - 7.34 (m, 2H), 7.07 - 7.16 (m, 1H), 6.91 (s, 1H), 5.04 (d, J = 6.8 Hz, 1H), 4.65 (s, 1H), 3.74 (s, 3H), 3.21 - 3.46 (m, 2H), 1.07 - 1.55 (m, 9H)

(B) Accurate mass measurement of Boc-IND by ESI-MS (Thermo Scientific™ Q Exactive™ hybrid quadrupole-Orbitrap mass spectrometer): $[C_{17}H_{22}N_2O_4Na = M+Na]^+$ theoretical: 341.1477, found 341.1476

(C) Chol-IND-Boc (4.50 g, 6.55 mmol, 32.3% yield) was obtained as a white solid, which was confirmed by 1H NMR: 400 MHz, $CDCl_3$, δ 7.58 (d, J = 8.0 Hz, 1H), 7.27 - 7.32 (m, 1H), 7.20 - 7.25 (m, 1H)[1], 7.08 - 7.14 (m, 1H), 6.87 (s, 1H), 5.34 (d, J = 3.6 Hz, 1H), 5.05 (d, J = 8.4 Hz, 1H), 4.53 - 4.67 (m, 2H), 3.75 (s, 3H), 3.27 (s, 2H), 2.22 (d, J = 7.6 Hz, 2H), 1.90 - 2.05 (m, 2H), 1.78 - 1.90 (m, 2H), 1.72 - 1.79 (m, 1H), 1.30 - 1.55 (m, 19H), 0.96 - 1.21 (m, 13H), 0.92 (d, J = 6.4 Hz, 4H), 0.88 (dd, J = 1.8, 6.8 Hz, 6H), 0.68 (s, 3H).

(D) Accurate mass measurement of Chol-IND-Boc by ESI-MS: $[C_{44}H_{66}N_2O_4Na = M+Na]^+$ theoretical: 709.4903, found 709.4912.

(E) Chol-IND-NH_2 free base (Chol-IND, 2.40 g, 4.09 mmol, 32.3% yield, 100% purity) was obtained as a white solid, which was confirmed by HPLC (Kinetex C18 column, 4.6 mm × 5.0 mm × 5 μm, mobile phase: [water (0.04% TFA)-MeCN]; B%: 50%-100%-50% MeCN, 4 min) temperature = 50°C, product: RT = 1.997 min, 100% purity at 220 nm) and 1H NMR: 400 MHz, $CDCl_3$, δ 7.64 (d, J = 8.0 Hz, 1H), 7.28 - 7.33 (m, 1H), 7.21 - 7.25 (m, 1H), 7.10 - 7.14 (m, 1H), 6.94 (s, 1H), 5.37 (d, J = 4.8 Hz, 1H), 4.56 - 4.72 (m, 1H), 3.71 - 3.85 (m, 4H), 3.27 (dd, J = 4.8, 14.4 Hz, 1H), 3.02 (dd, J = 7.6, 14.4 Hz, 1H), 2.27 - 2.29 (m, 2H), 1.95 - 2.08 (m, 2H), 1.74 - 1.92 (m, 3H), 1.04 - 1.65 (m, 20H), 0.95 - 1.03 (m, 6H), 0.93 (d, J = 6.4 Hz, 3H), 0.88 (dd, J = 2.0, 6.8 Hz, 6H), 0.69 (s, 3H). Accurate mass measurement of Chol-IND by ESI-MS: $[C_{39}H_{59}N_2O_2 = M+H]^+$ theoretical: 587.4576, found 587.4522 (shown in **Figure 3C**).

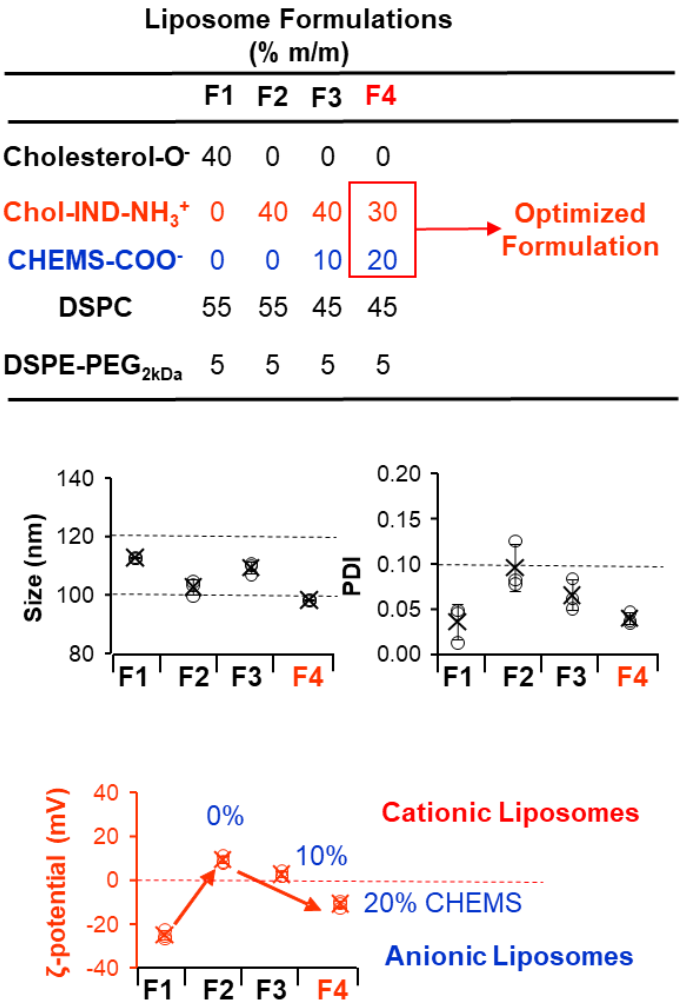

Figure S2. Optimizing the zeta potential of the L-MTO/IND formulation through the use of cholesterol hemisuccinate (CHEMS). We experimented with four different formulations, F1-4. F1 was a standard liposomal formulation that closely resembled clinically approved Doxil®. F1 was comprised of 40% cholesterol with no Chol-IND nor CHEMS, yielding liposomes sized around 100-120 nm, with a low polydispersity index (PDI < 0.1) and a negative ζ-potential. F2 replaced cholesterol with Chol-IND, resulting in ~100 nm liposomes (PDI < 0.1) in which ζ-potential was ~+10 mV. To neutralize the cation charge introduced by Chol-IND, we made use of the negatively charged COO^- group in CHEMS. F3 reduced the DSPC content by 10% mm to accommodate CHEMS at an equal molar ratio, yielding liposomes with the appropriate size and PDI, but showing almost neutral ζ-potential ~ +3mV. In order to achieve a more negative ζ-potential, Chol-IND was reduced to 30% m/m, while CHEMS was increased to 20% m/m. This yielded F4, in which liposomes ~100 nm, a narrow PDI, and negative ζ-potential of -10 mV was obtained. F4 was subsequently used as the most desirable formulation in animal studies. In addition to the charge neutralization effect, paired use of Chol-IND/CHEMS introduced a pH-dependent charge variation effect, which is further discussed in the main manuscript as Fig. 4C.

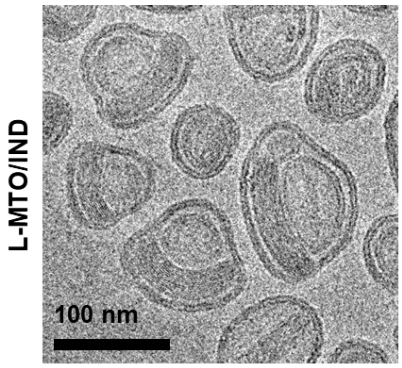

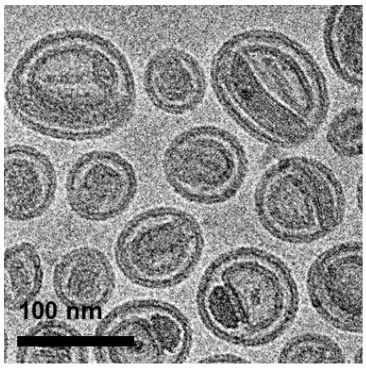

Day 0	
Hydrodynamic size (nm) (PDI)	97.2 ± 3.5
Polydispersity Index (PDI)	0.096
ζ-potential (mV)	-5.73 ± 1.48

3-month storage at 4°C in PBS	
Hydrodynamic size (nm)	93.5 ± 1.3
Polydispersity Index (PDI)	0.089
ζ-potential (mV)	-9.16 ± 0.90
Free IND concentration (μg/mL)	1.15 ± 0.10
IND Cleavage (%)	0.88 ± 0.08
Free MTX (%)	0.06 ± 0.03

Figure S3. Three-month stability data for the L-MTO/IND liposome. Freshly prepared L-MTO/IND at 2 mM was stored in PBS at 4°C and pH 7.4 for 3-months. No significant changes in liposomal morphology as well as colloidal stability (hydrodynamic size, polydispersity index, and zeta potential), as confirmed by cryoEM and dynamic light scattering. MTO leakage and release of soluble IND by prodrug cleavage were both below 1% upon HPLC analysis. This shows the development of a stable liposomal formulation.

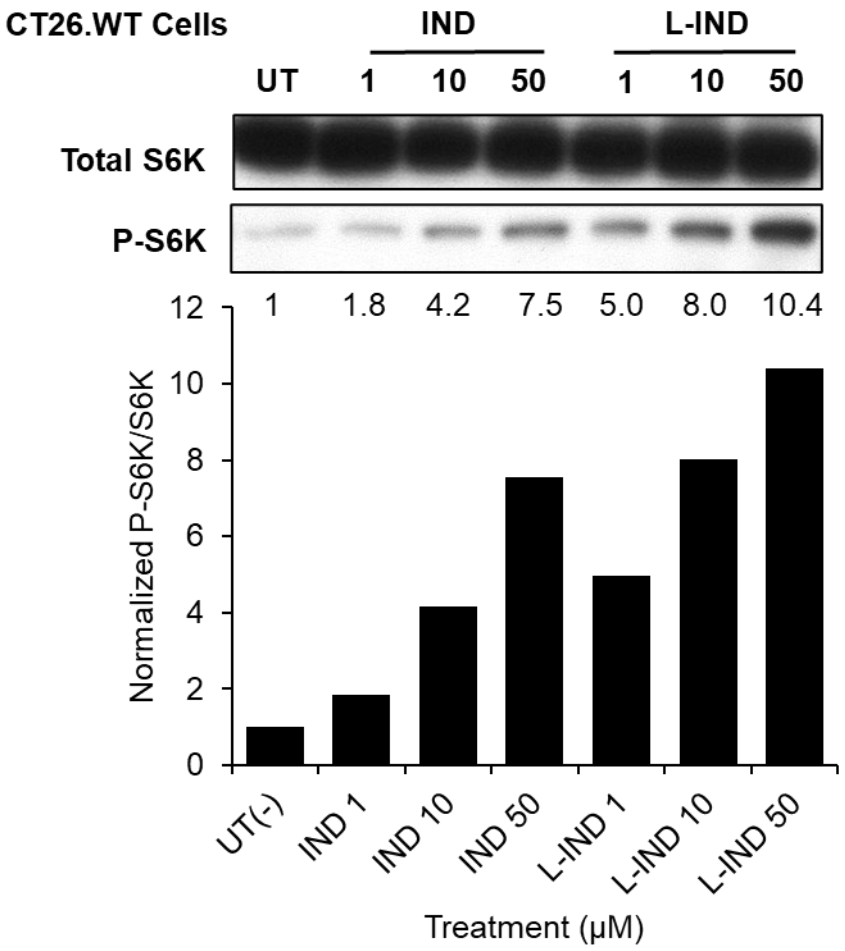

Figure S4. *In Vitro* study of liposomal Chol-IND (L-IND) on phospho-S6K CT26 cells were pre-treated with IFN-γ (100 ng/mL) overnight to stimulate IDO expression. Cells were incubated in serum-free and tryptophan-free cell culture media supplemented with either free IND or L-IND (liposomal Chol-IND) at 1, 10, and 10 μM for 6 h. Western blotting of the P-S6K v.s. total S6K ratios were used as an indicator of activated downstream of mTOR.

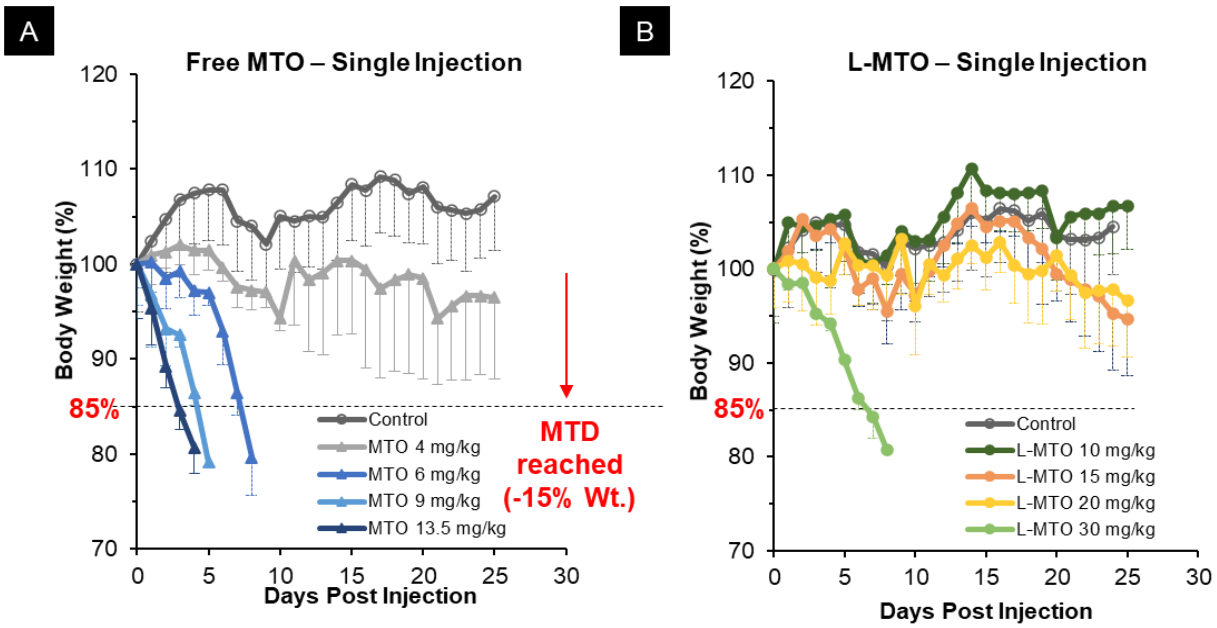

Figure S5. Estimation of the maximum tolerated dose (MTD) for MTO. (A) In order to determine the MTD dose for Balb/c, our starting MTO dose was designed based on the literature.[2] Doses were escalated until reaching the MTD, *i.e.,* 15% body weight loss. For free drug treatment, we observed rapid body weight loss at 6 mg/kg; free drug MTD was estimated at 3 mg/kg. (B) . The MTD value of liposomal MTO was estimated to be ~20 mg/kg (MTO dose), based on the finding that no significant weight loss was seen at this dose, but animals receiving 30 mg/kg that weight loss> 15%. In summary, the MTO toxicity is dose-dependent, which can be significantly mitigated by liposomal formulation.[3]

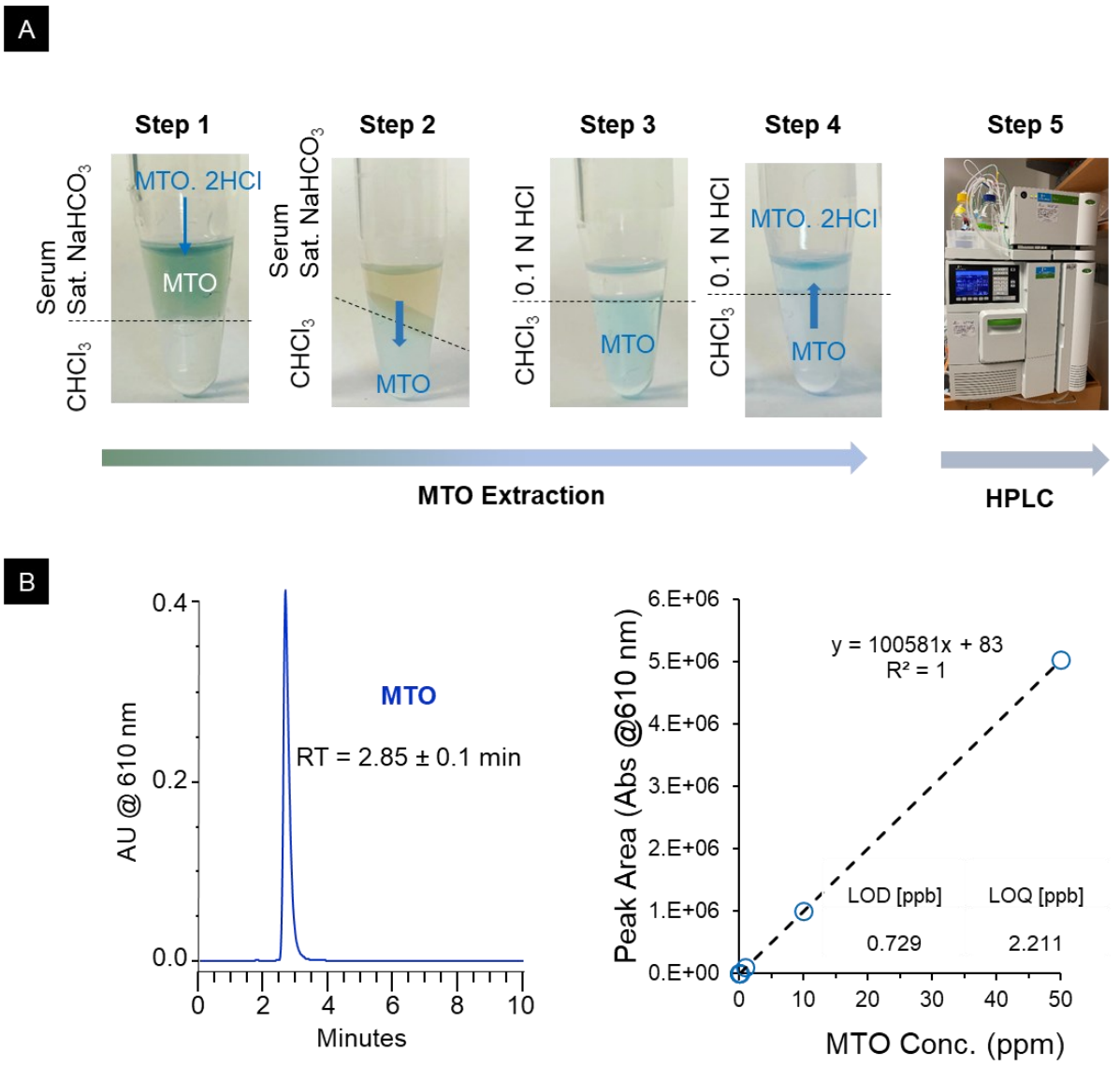

Figure S6. Use of HPLC to determine the pharmacokinetic profile of MTO. (A) The extraction of mitoxantrone dihydrochloride salt (MTO•2HCl) started by naturalizing the salt with saturated sodium bicarbonate ($NaHCO_3$) solution. The generated MTO free base was then isolated by micro-extraction against chloroform ($CHCl_3$, lower phase), as shown in step 1-2. To prepare the extracted MTO in an HPLC compatible solvent, free base MTO in $CHCl_3$ was back-extracted by 0.1N HCl solution, leading to MTO•2HCl as an aqueous solution (step 4, upper phase). The MTO•2HCl solution was filtered (0.45 µm pores), followed by HPLC analysis (step 5). (B) The chromatogram of MTO was acquired by PerkinElmer Altus HPLC with a Brownlee SPP 2.7 µm C18 Columns (4.6 X 150 mm). Mobile phase: 10 mM sodium phosphate buffer (pH 2.3) with 0.1 % triethylamine (mobile phase A) and acetonitrile (mobile phase B) at fixed ratio of = 81:19 (v/v), flow rate of 1 mL/min at 25°C, detected by UV at 610 nm with a retention time 2.85 ± 0.1 min. (C) The limit of detection of quantification (LOD/LOQ) of the MTO by the HPLC method mentioned above.

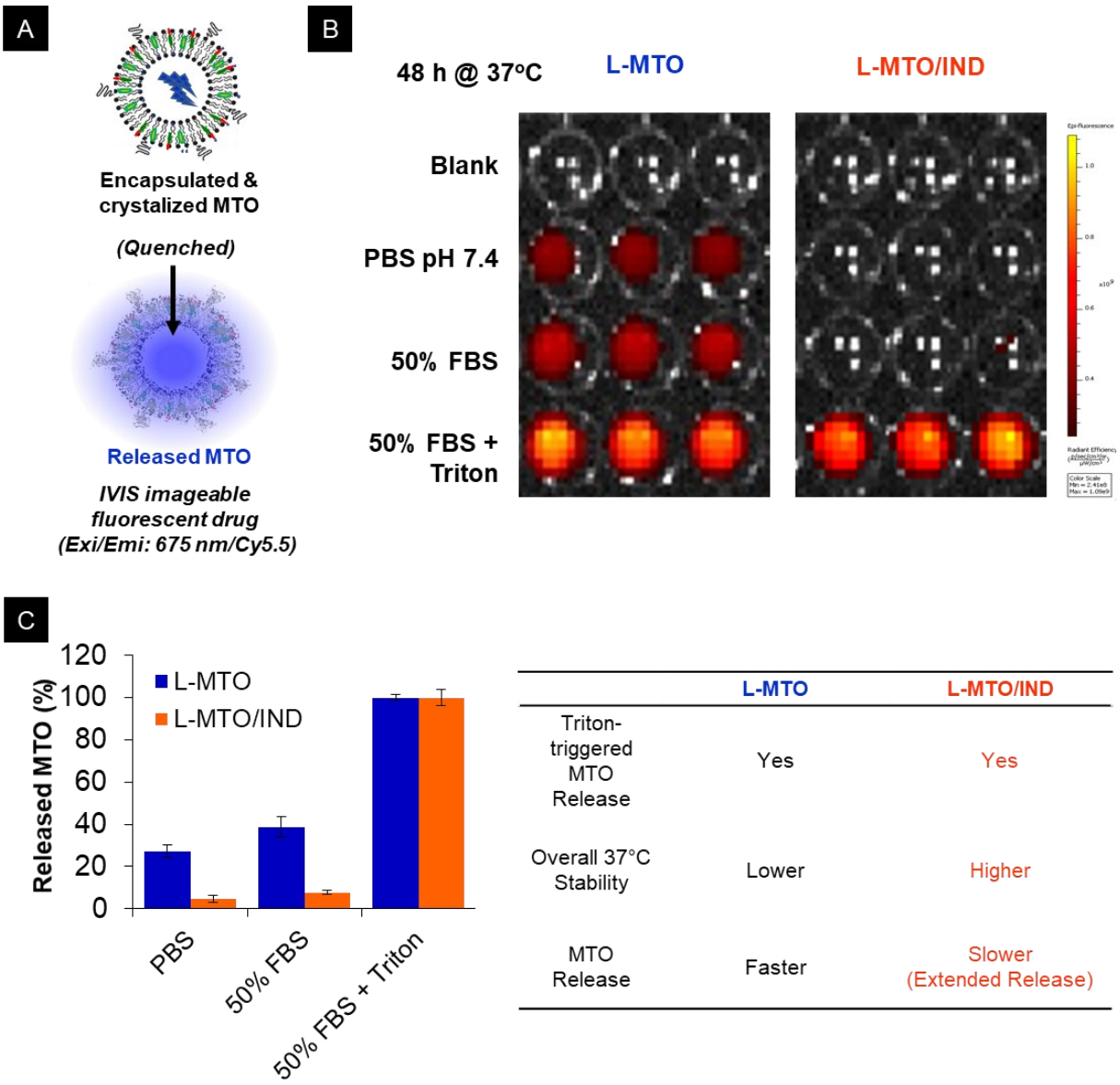

	L-MTO	L-MTO/IND
Triton-triggered MTO Release	Yes	Yes
Overall 37°C Stability	Lower	Higher
MTO Release	Faster	Slower (Extended Release)

Figure S7. Fluorescent properties of liposomal encapsulated (quenched) and released MTO (A) Schematic illustration to illustrate quenching of encapsulated MTO, which is reversed upon release of soluble MTO from the carrier. (B). IVIS imaging to visualize MTO release following incubation in PBS over 48 h at 37° at pH 7.4. The release in the presence of PBS alone is compared to the effect of 50% FBS, as well as treatment with Triton-X100. Samples were imaged in a 96-well plate and visualized by an IVIS imager (Exi/Emi = 675 nm/Cy5.5). (C) Quantification of the released MTO by measuring fluorescence radiance efficiency. The overall comparison between the L-MTO and L-MTO/IND is summarized in the lower right table.

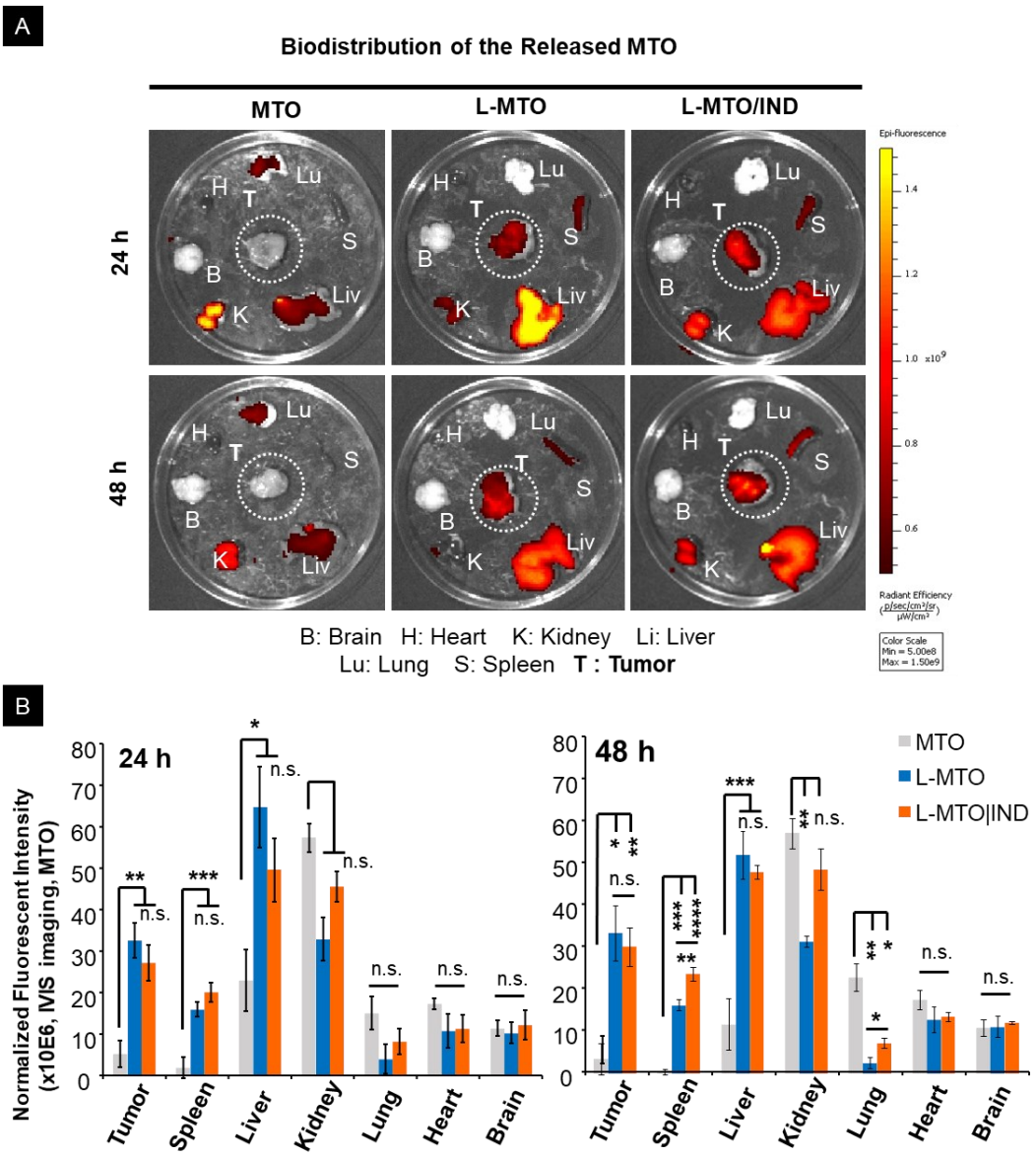

Figure S8. Use of IVIS imaging to visualize released MTO in mice receiving i.v. injection of MTO. (A) Animals biodistribution studies: Mice were i.v. injected with an MTO dose equivalent of 3 mg/kg free drug, L-MTO, and L-MTO/IND. Animals were sacrificed after 24 h (Figure S4) or 48 h, followed by explant of the tumors and major organs in a Petri dish for quantitative IVIS imaging. (B) The normalized fluorescence radiance efficiency of (A) is shown and compared at 24 h and 48 h post i.v. injection. MTO fluorescence intensity was expressed as the average normalized value of the radiant efficiency [p/s/cm²/sr]/[μW/cm²] × 10E^6)] resulting from drug release from liposomes. Data were expressed as mean ± SD, n = 3. (ANOVA, post hoc = Tukey's: *p<0.05; **p < 0.01, ***p < 0.001, ****p < 0.001, n.s. p > 0.05).

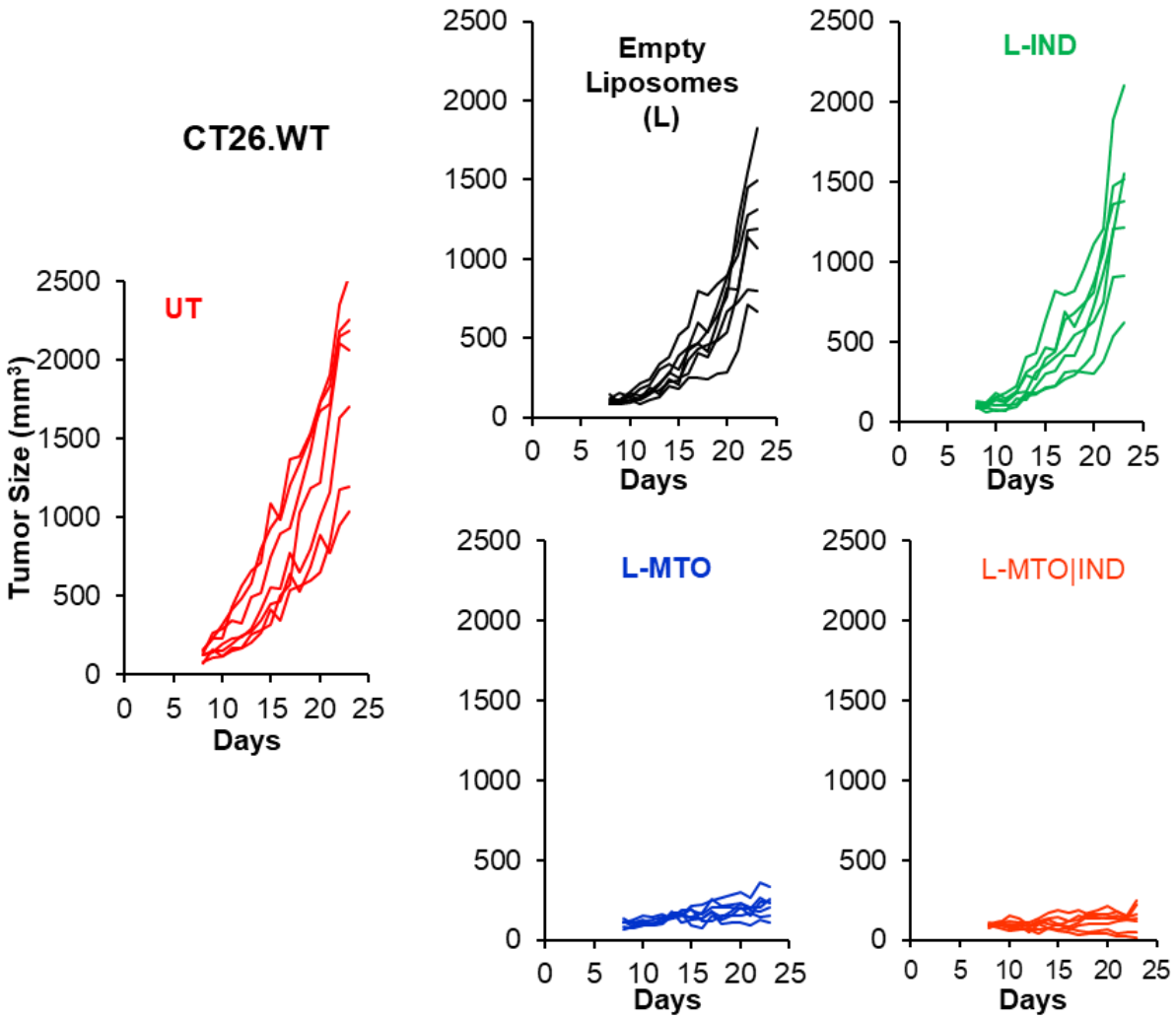

Figure S9. Individual tumor growth curves in the CT26 efficacy study. The data were present as "spaghetti plots" that display the tumor growth in each animal. This demonstrated that tumor growth approached the point of disappearance for several animals in the L-MTO/IND treatment group. These data correspond to the experiment shown in Fig. 6.

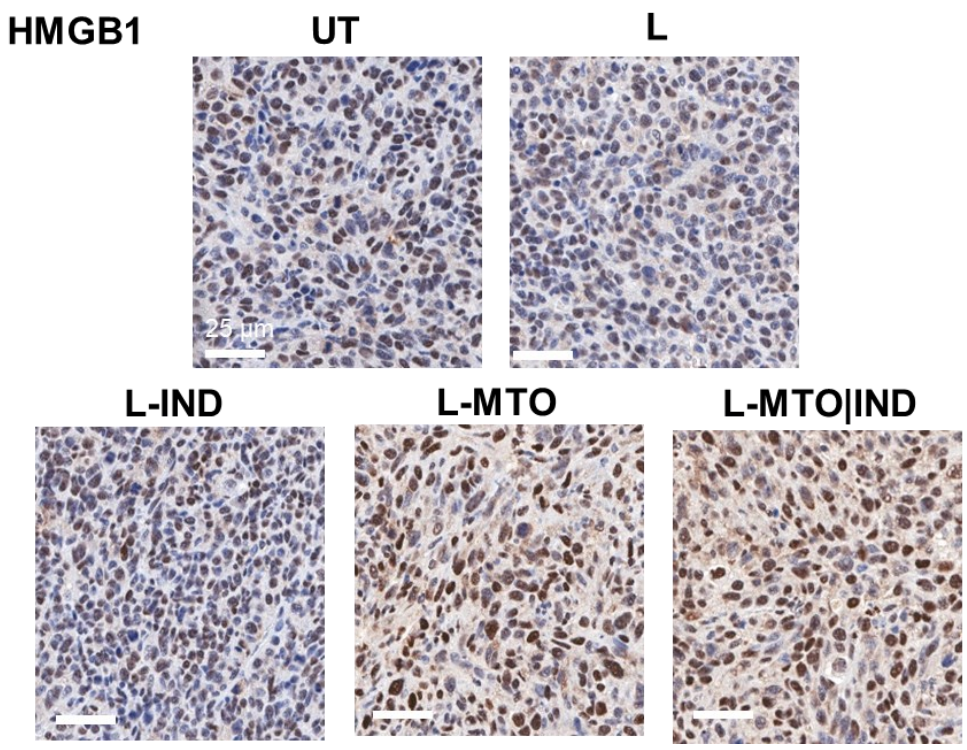

Figure S10. Representative IHC staining for HMGB1 in CT26 tumors. Tumors were harvested from the 23-day efficacy study, described in Fig. 6.

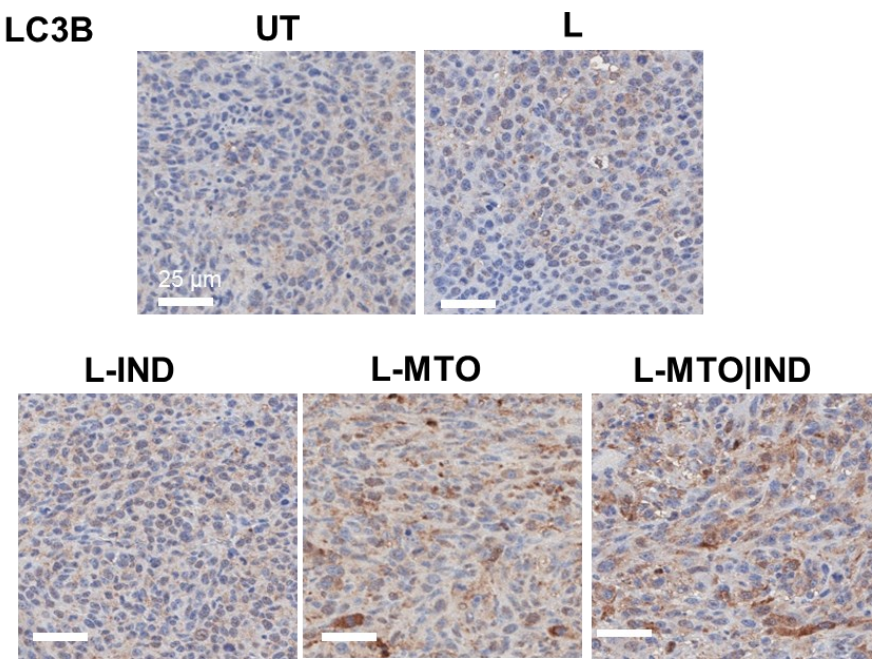

Figure S11. Representative IHC staining for LC3B in CT26 tumors.

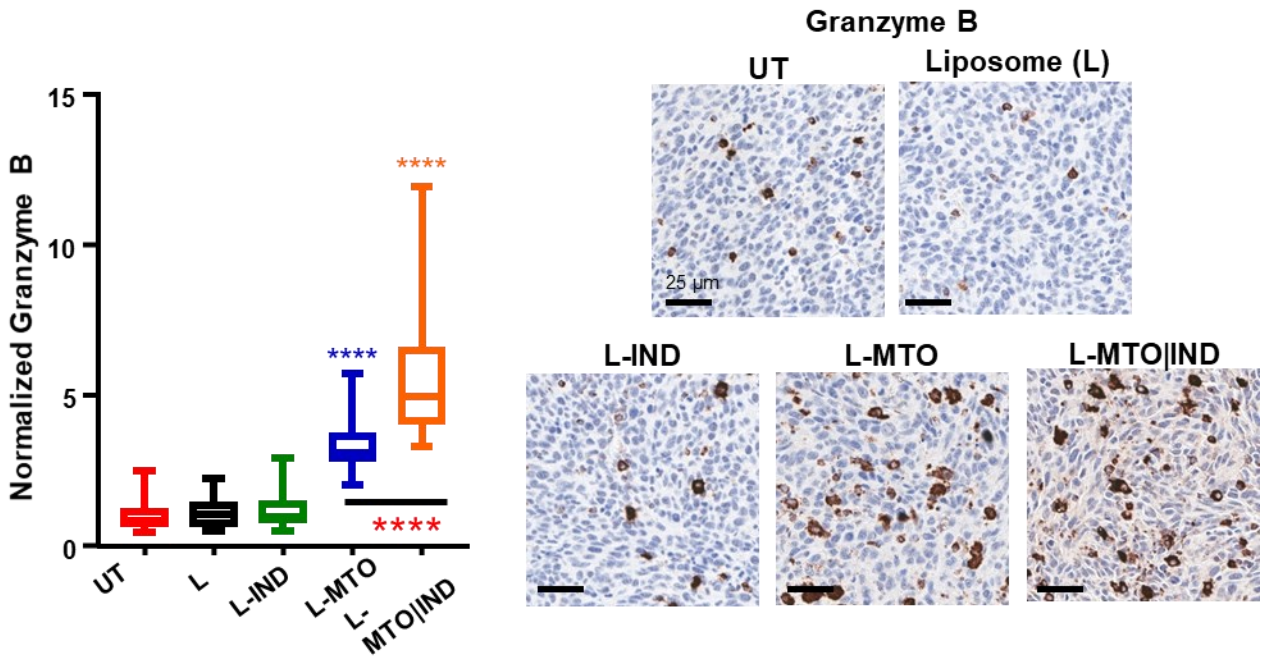

Figure S12. Immune phenotyping to demonstrate the effect of L-MTO/IND on inducing granzyme B release. Quantification and representative IHC staining images for granzyme B expression, demonstrating that the L-MTO/IND liposome was able to trigger a more effective release of this cytotoxic compound when compared to L-MTO. (****$p < 0.0001$, ANOVA). These data were collected in the efficacy study, described in Fig.6, and likely reflect, granzyme B release from NK cells, as suggested in Figures. 7D and 7E.

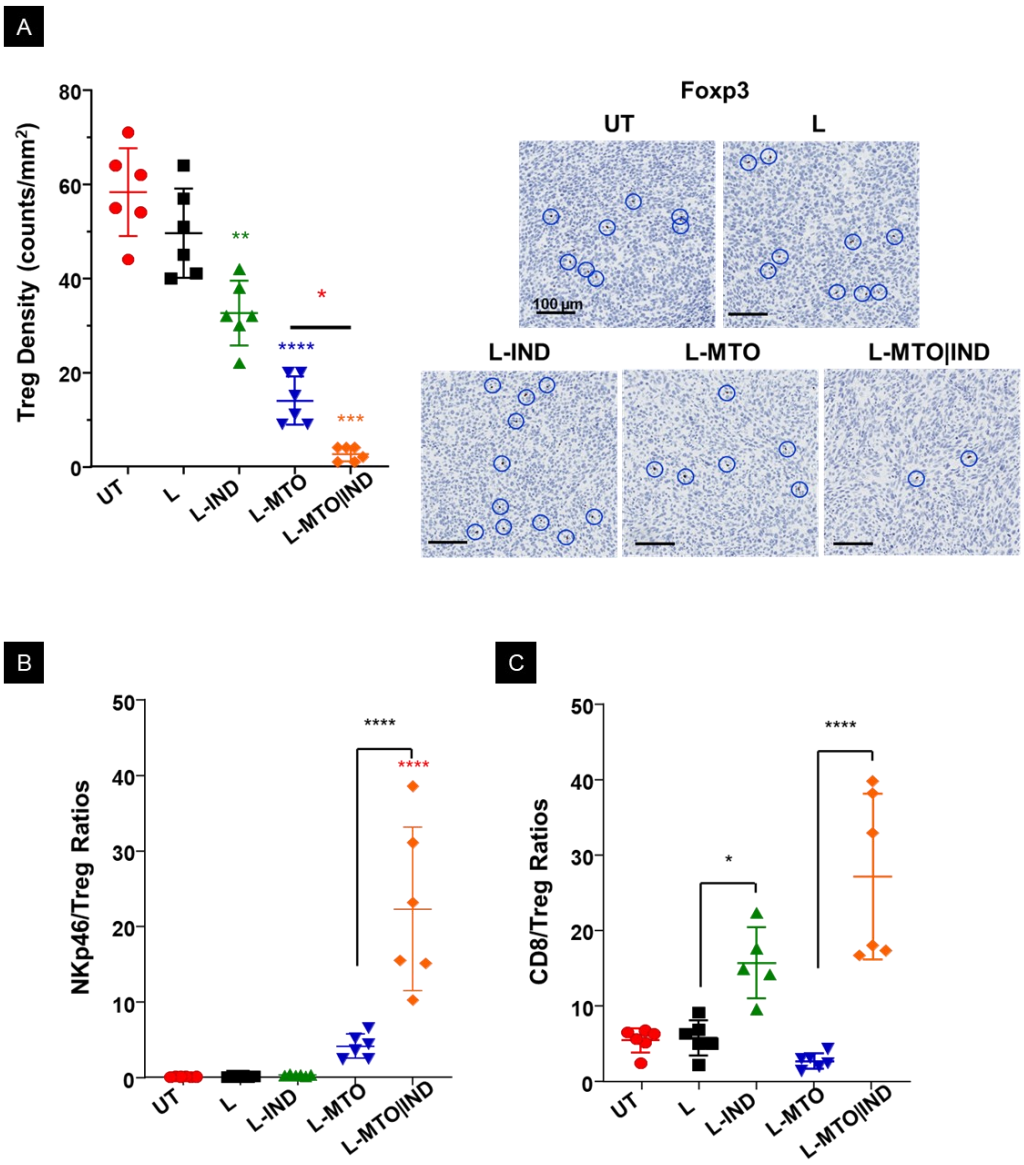

Figure S13. Representative IHC staining for Foxp3, the NK/Treg, and CD8/Treg rations in CT26 tumors. (A) Both L-IND and L-MTO could effectively reduce the number of Foxp3^{+} Tregs, particularly L-MTO/IND. Six ROIs were included in the analysis. (B-C) The combined use of Treg (Fig. S13A), CD8 (Fig. 7C), and NK (Fig. 7D) quantification to calculate NK/Treg and CD8/Treg ratios. These data were obtained from CT26 tumors collected in the efficacy study, described in Fig. 6. (B) The NKp46/Treg ratios (n = 6) were dramatically increased (ANOVA post hoc = Turkey's test, ****p < 0.0001) (C) The CD8/Treg ratios (n = 6) showed significantly increased ratios for L-IND and L-MTO/IND (ANOVA, post hoc = Tukey's test, *p < 0.05, ****p < 0.0001).

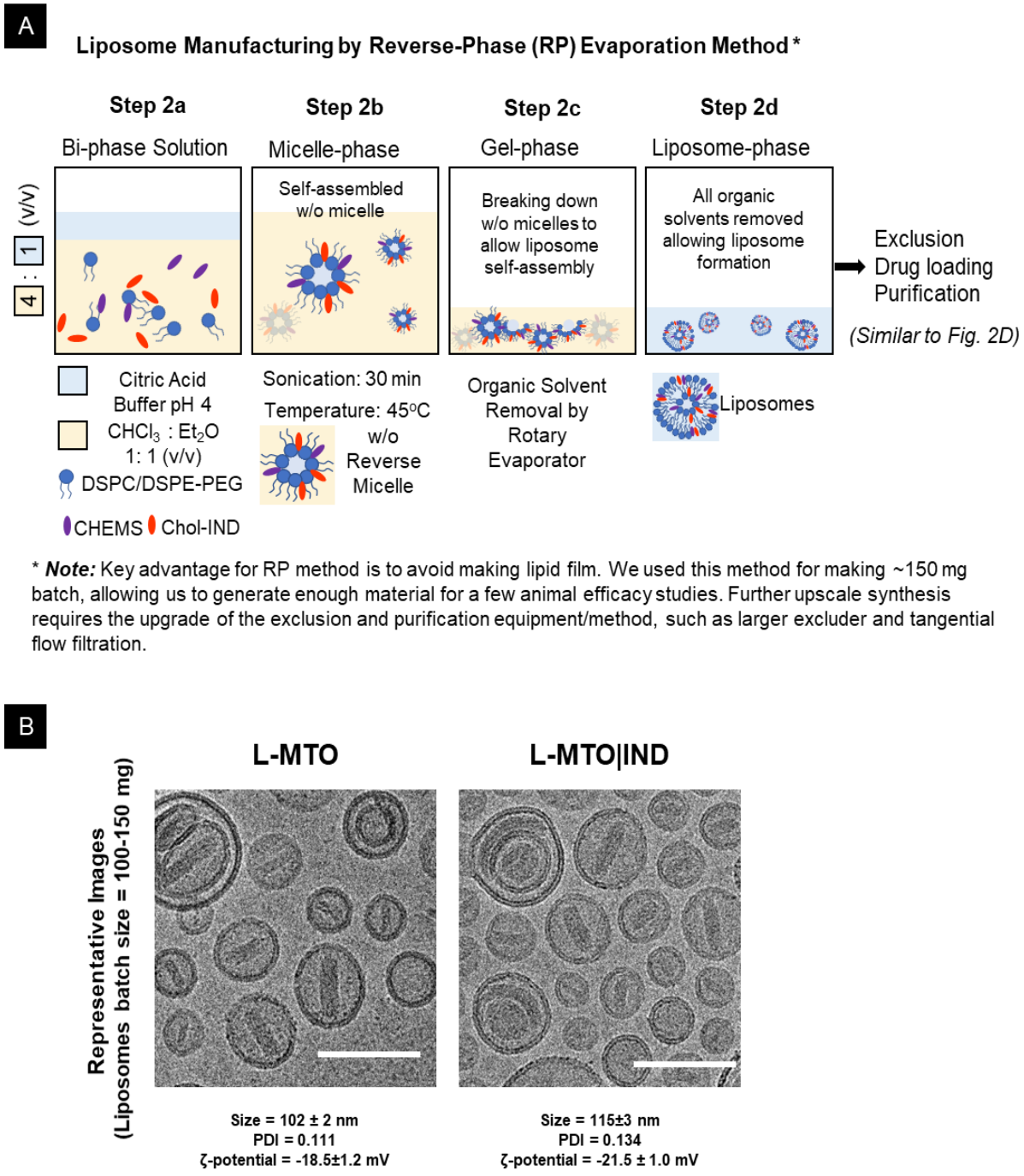

Figure S14. Liposome manufacturing using a reverse-phase evaporation method. (A) Schematic illustration of the reverse phase evaporation method for liposome manufacturing. (B) CryoEM micrographs demonstrated comparable morphologies for L-MTO (RP) and L-MTO/IND (RP) compared to the liposomes produced by the lipid film method. The liposomal physicochemical characteristics are shown below each CryoEM picture.

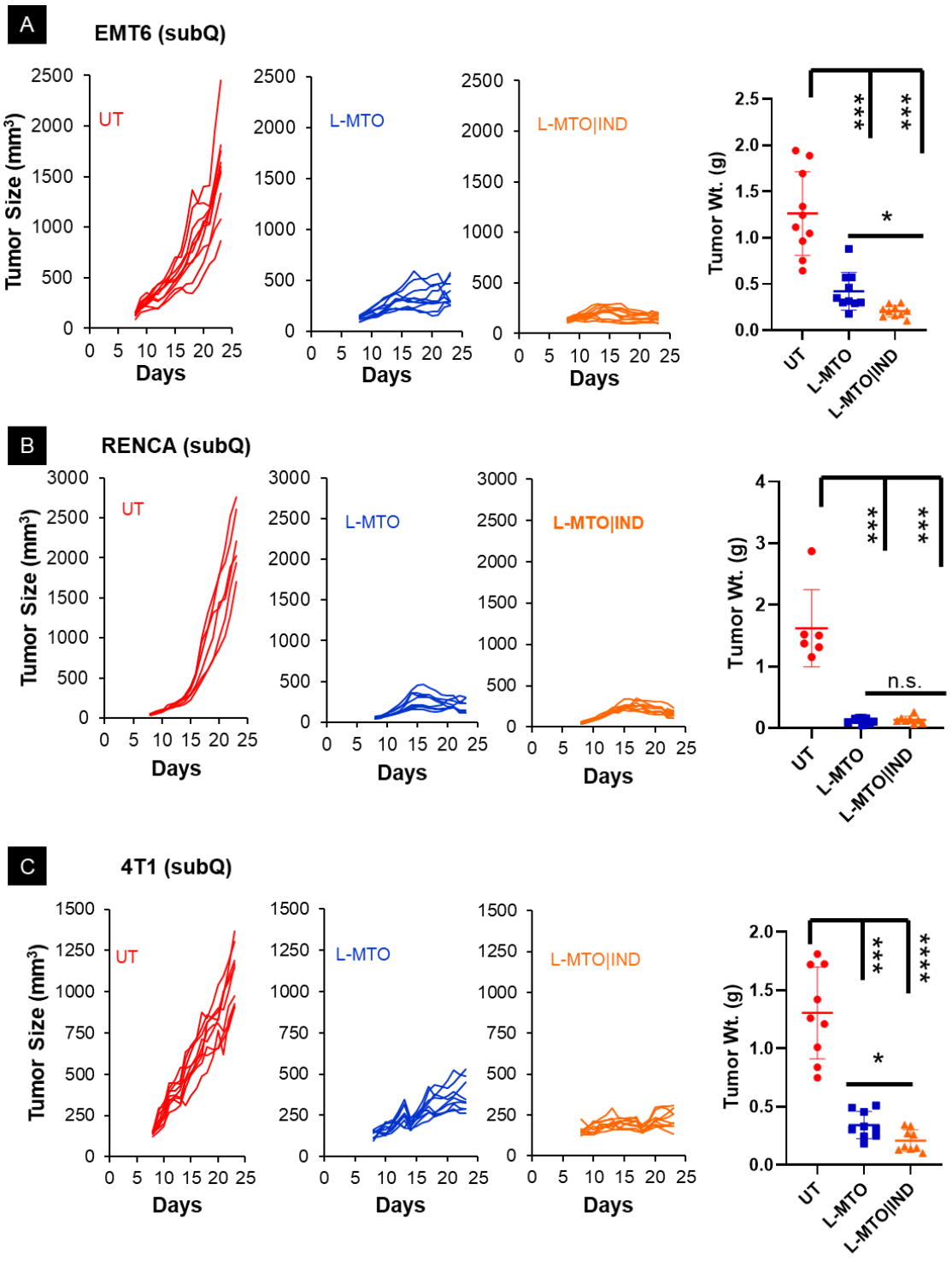

Figure S15. Individual tumor growth curves and tumor weight measurements for the EMT6 (A), RENCA (B), and 4T1 (C) efficacy studies. These data correspond to the data shown in Figure. 10. (*p < 0.05, ***p < 0.001, ****p < 0.0001, ANOVA).

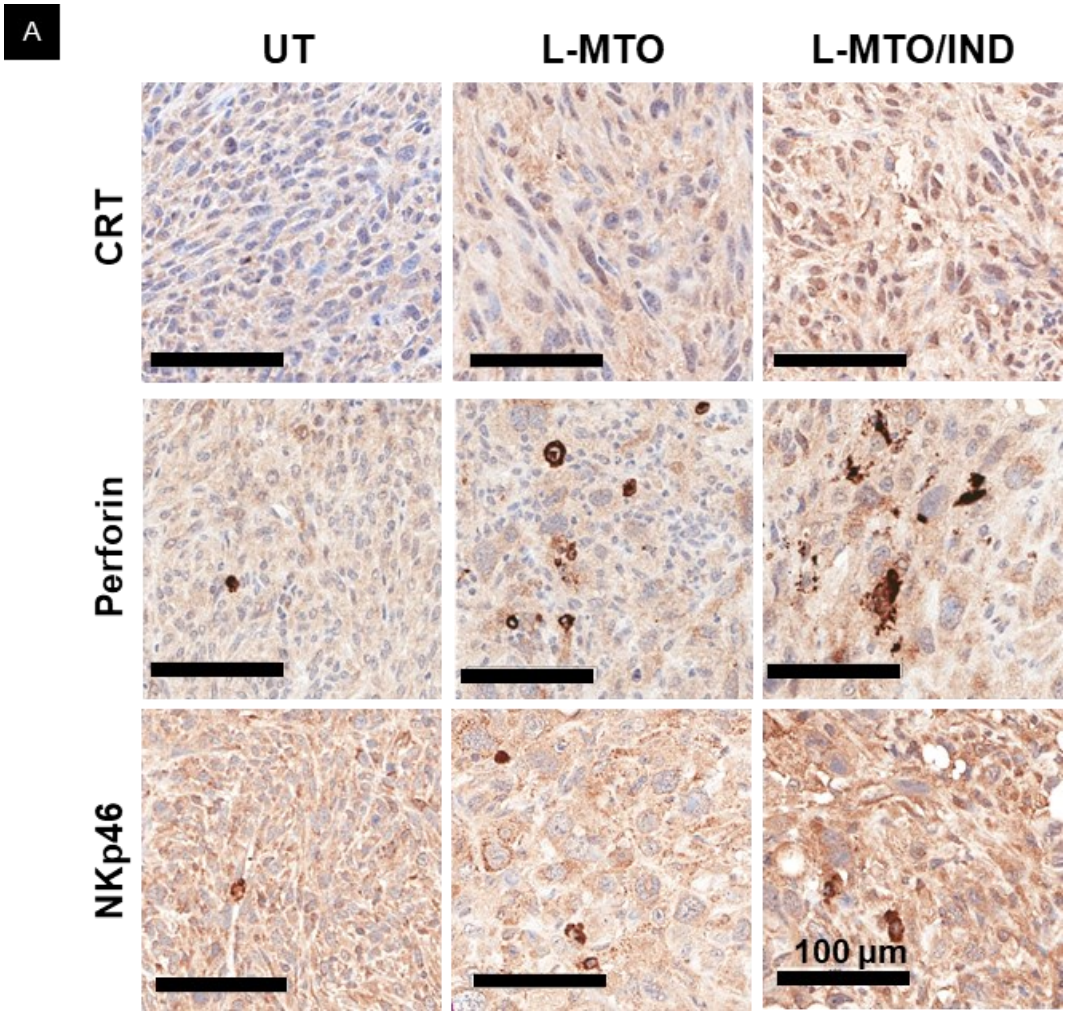

Figure S16A. Representative IHC staining for CRT, perforin, and NKp46, in (A) subcutaneous EMT6 tumors harvested from the 23-day efficacy study (Figure 10A/S11A).

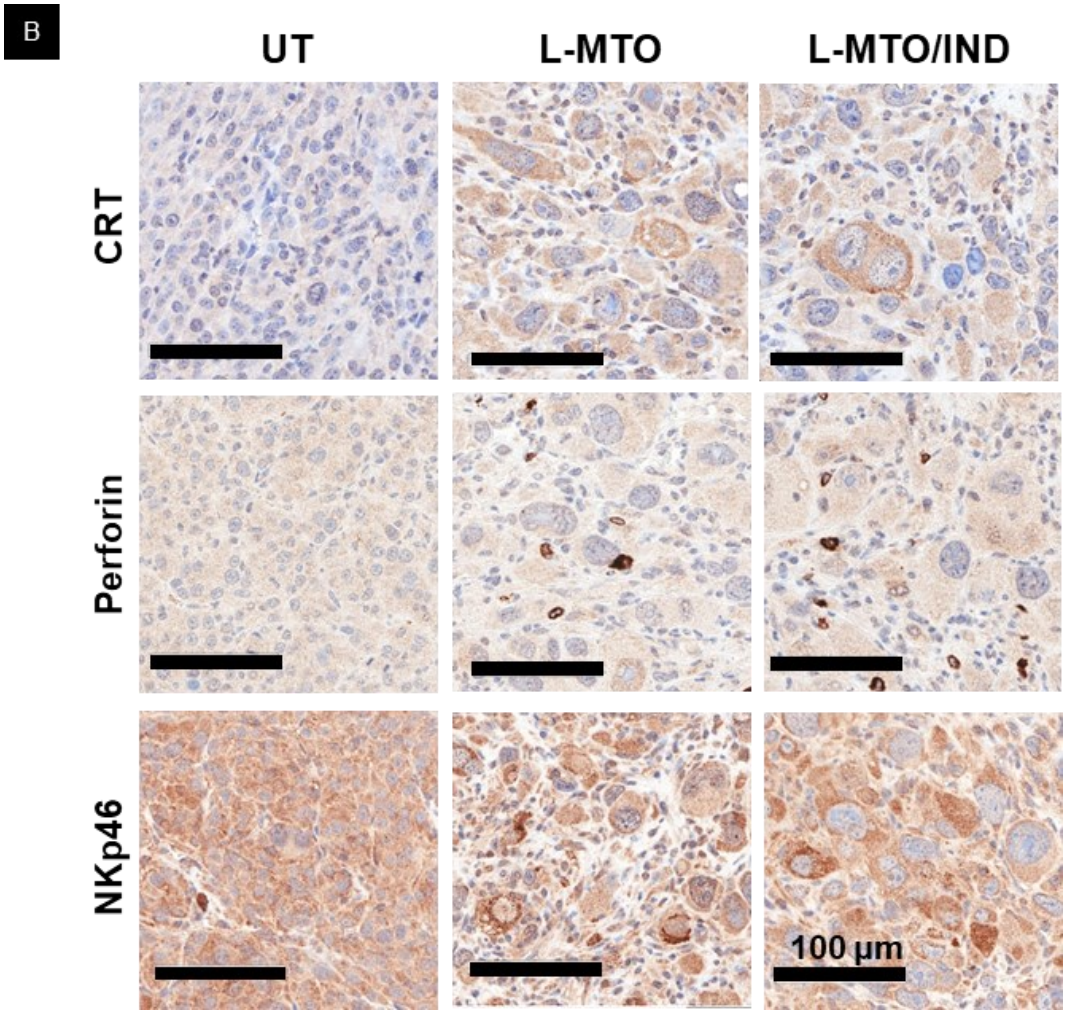

Figure S16B. Representative IHC staining for CRT, perforin, and NKp46, in (B) subcutaneous RENCA tumors harvested from the 23-day efficacy study (Figure 10B/S11B). (*$p < 0.05$, **$p < 0.01$, ****$p < 0.0001$, ANOVA).

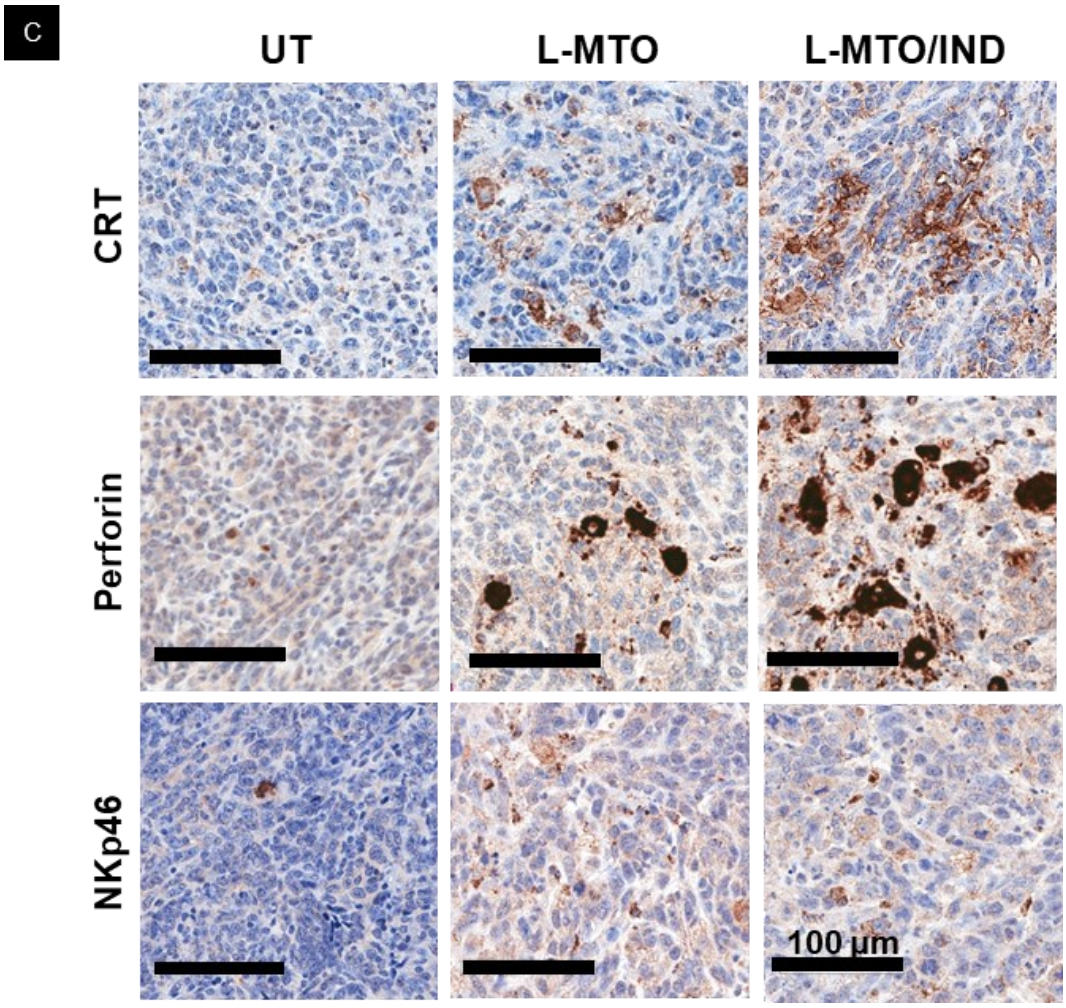

Figure S16C. Representative IHC staining for CRT, perforin, and NKp46, in (C) subcutaneous 4T1 tumors harvested from the 23-day efficacy study (Figure 10C/S11C).

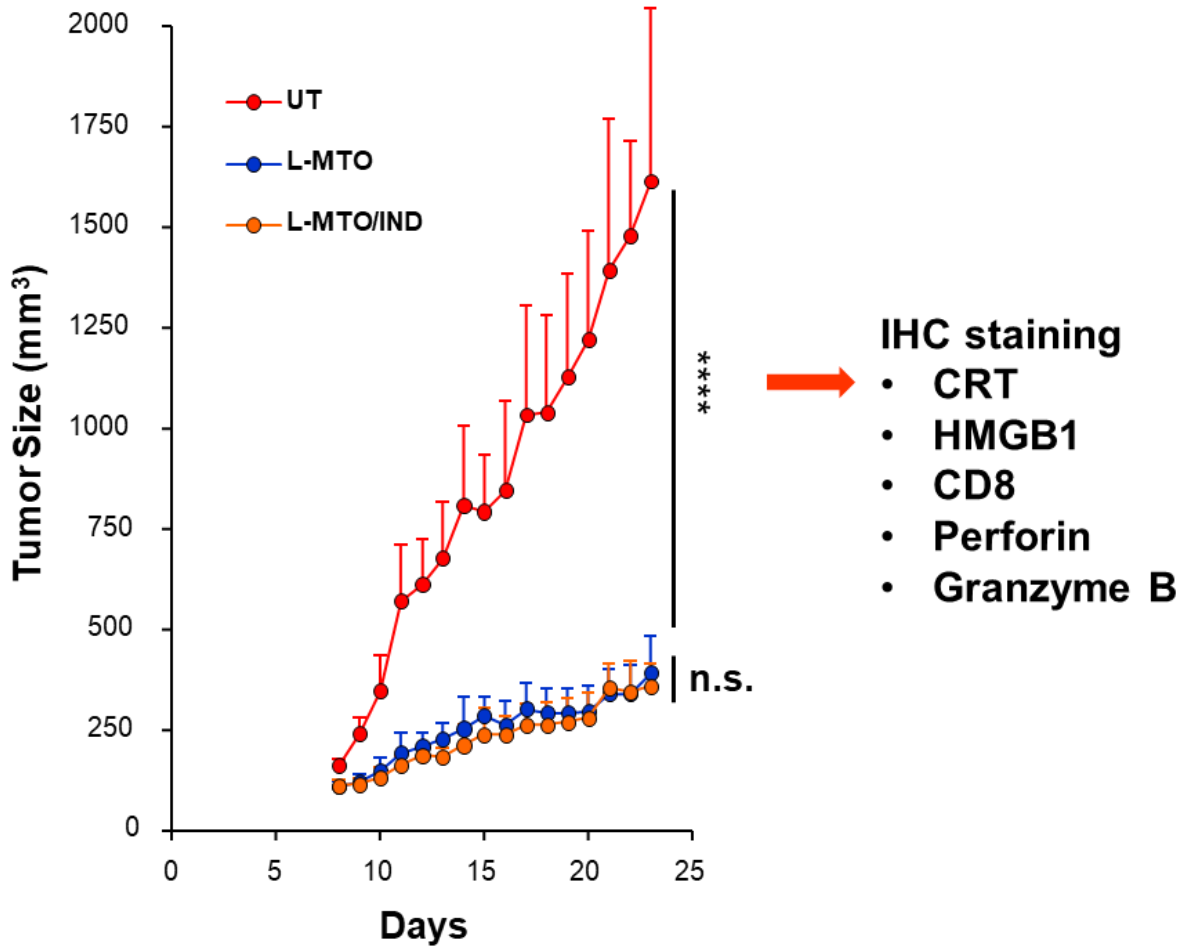

Figure S17. Efficacy study in the 4T1 orthotopic tumor model concluded on day 23 followed by tumor harvesting and performance of IHC analysis for the response parameters shown on the right-hand side. Data for the IHC analysis appear in Fig. S13. (****$p < 0.0001$, ANOVA).

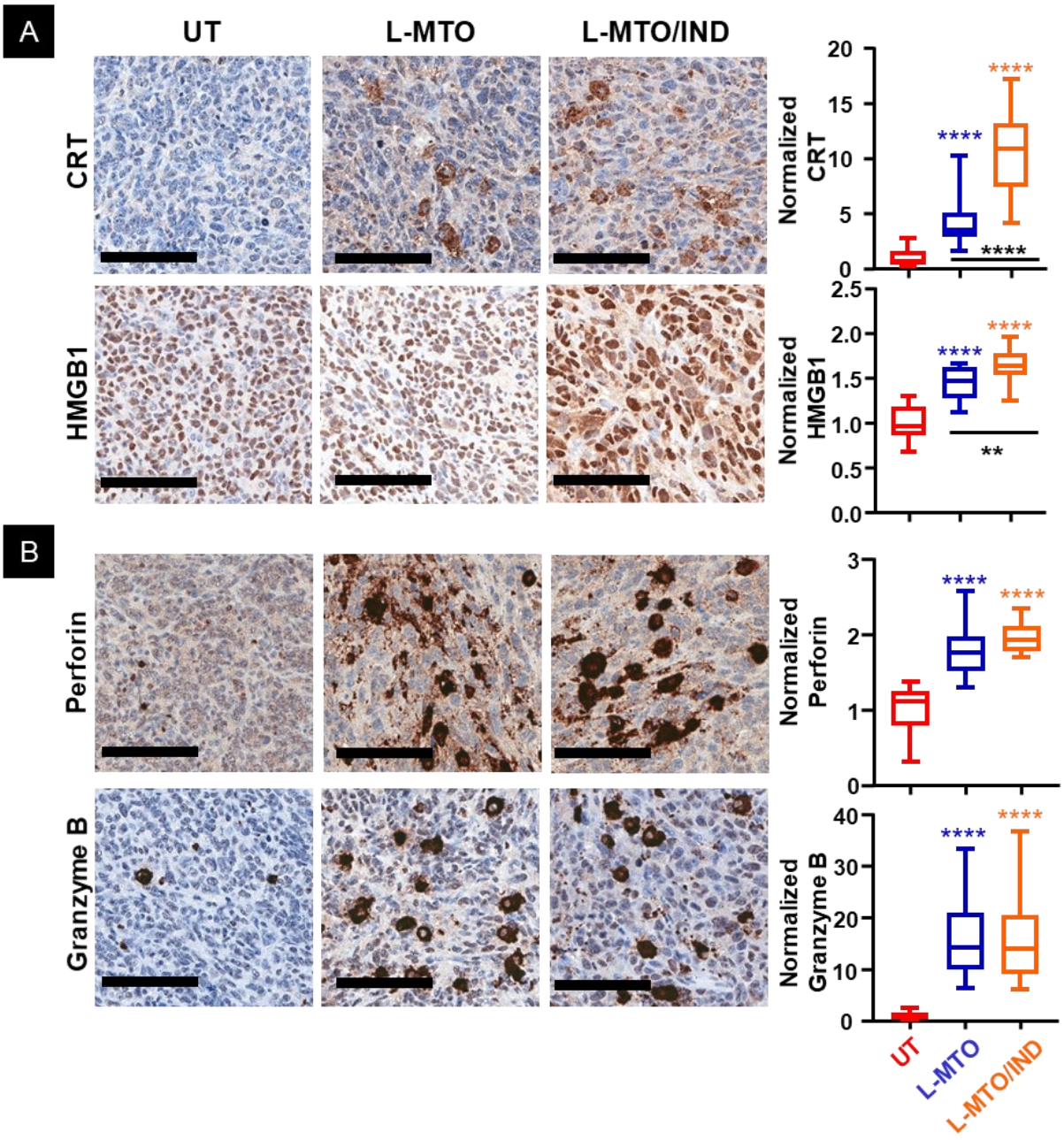

Figure S18A-B. Representative IHC staining and quantification for (A) CRT and HMGB1 (B) perforin and granzyme B in orthotopic 4T1 tumors harvested from the 23-day efficacy study (Figure S12). (ANOVA, post hoc Tukey's test, adjusted $^{**}p < 0.01$, $^{****}p < 0.0001$).

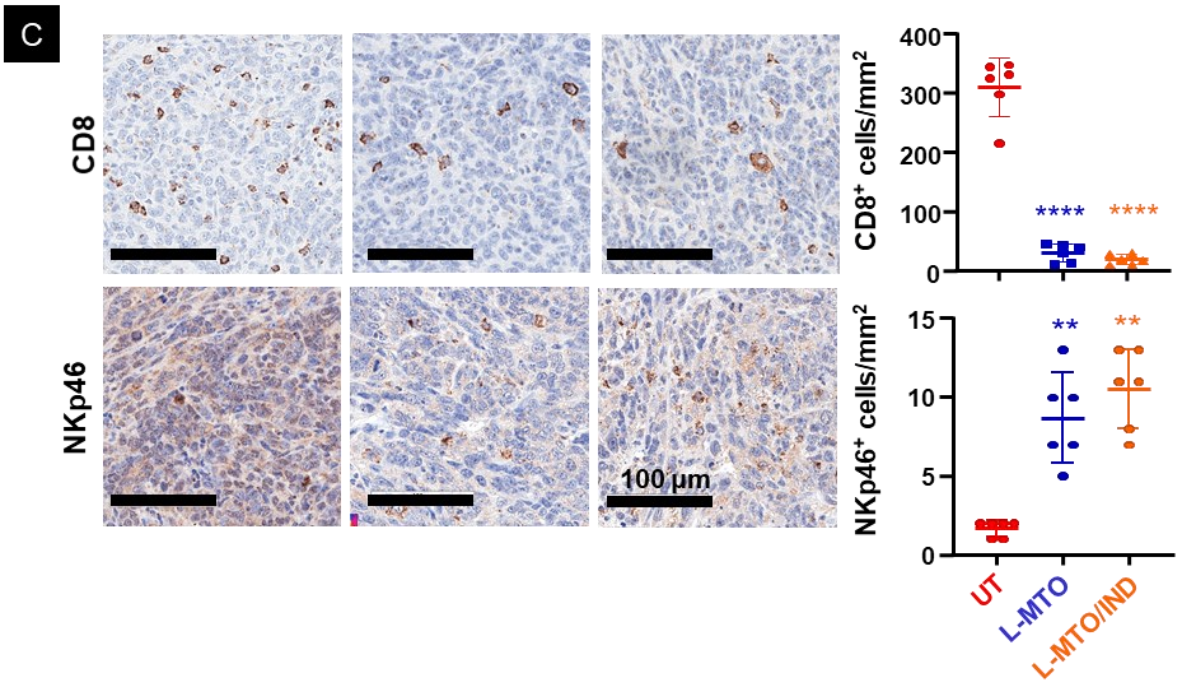

Figure S18C. Representative IHC staining and quantification for (C) CD8 and NKp46 in orthotopic 4T1 tumors harvested from the 23-day efficacy study (Figure S12).

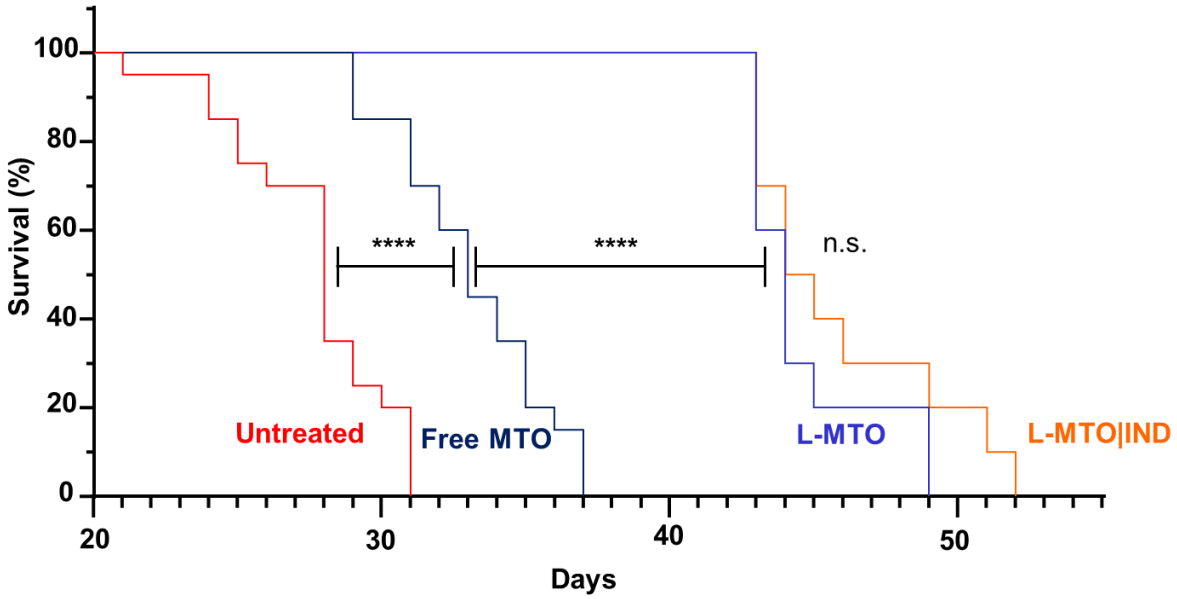

Figure S19. Survival study in a 4T1 orthotopic tumor model. A survival study was undertaken based on the significant response differences between L-MTO and L-MTO/IND in the subcutaneous efficacy study shown in Figure 10E. The 4T1 orthotopic model was established by injection of 0.7M 4T1 cells subcutaneously into the 2nd right mammary fat pad of female Balb/c mice. When tumor sizes reached ~100 mm^3, animals were treated with saline (as untreated control, n = 20), free MTO (1 mg/kg × 3 injections, n = 20), L-MTO (3 mg/kg × 3 injections, n = 10) and L-MTO/IND (3 mg/kg × 3 injections, n = 10) through tail vein i.v. injections every 3 days. Kaplan-Meier analysis shows a median survival of 28, 33, 44, and 44.5 days for untreated, MTO, L-MTO, and L-MTO/IND treated groups, respectively. While free MTO significantly improved animal survival when compared to the untreated group (Log-rank test, Chi-square 28.47, p < 0.0001). Further improvement from free MTO was achieved using the liposomal formulations (L-MTO v.s. MTO, Log-rank test, Chi-square 24.75, p < 0.0001). IND co-delivery with MTO trended towards longer survival, but the results were not non-statistically significant compared to L-MTO in this orthotopic model (Log-rank test, Chi-square 1.211, p = 0.2712).

Competing financial interests

Andre E. Nel and Huan Meng are co-founders and equity holders in Westwood Biosciences Inc. and NAMMI Therapeutics. Nel and Meng also serve on the Board for Westwood Biosciences Inc. The remaining authors declare no conflicts of interest.

References

1. Pol, J.; Vacchelli, E.; Aranda, F.; Castoldi, F.; Eggermont, A.; Cremer, I.; Sautès-Fridman, C.; Fucikova, J.; Galon, J.; Spisek, R.; Tartour, E.; Zitvogel, L.; Kroemer, G.; Galluzzi, L., Trial Watch: Immunogenic Cell Death Inducers for Anticancer Chemotherapy. *Oncoimmunology* **2015,** *4*, e1008866-e1008866.
2. Li, C.; Cui, J.; Li, Y.; Wang, C.; Li, Y.; Zhang, L.; Zhang, L.; Guo, W.; Wang, J.; Zhang, H.; Hao, Y.; Wang, Y., Copper Ion-Mediated Liposomal Encapsulation of Mitoxantrone: The Role of Anions in Drug Loading, Retention and Release. *European Journal of Pharmaceutical Sciences* **2008,** *34*, 333-344.
3. Chang, C. W.; Barber, L.; Ouyang, C.; Masin, D.; Bally, M. B.; Madden, T. D., Plasma Clearance, Biodistribution and Therapeutic Properties of Mitoxantrone Encapsulated in Conventional and Sterically Stabilized Liposomes After Intravenous Administration in BDF1 Mice. *British Journal of Cancer* **1997,** *75* (2), 169-177.